Charge Transport and Structure in Semimetallic Polymers

Sam Rudd,[1] Juan F. Franco-Gonzalez,[2] Sandeep Kumar Singh,[2] Zia Ullah Khan,[2] Xavier Crispin,[2] Jens W. Andreasen,[3] Igor Zozoulenko,[2] Drew Evans[1]

[1]Thin Film Coatings Group, Future Industries Institute, University of South Australia, Mawson Lakes, South Australia 5095, Australia
[2]Department of Science and Technology, Organic Electronics, Linkoping University, Norrkoping SE-601 74, Sweden
[3]Department of Energy Conversion and Storage, Frederiksborgvej 399, Technical University of Denmark, Roskilde 4000, Denmark
Correspondence to: D. Evans (E-mail: drew.evans@unisa.edu.au)

Received 20 April 2017; accepted 3 October 2017; published online 16 October 2017
DOI: 10.1002/polb.24530

ABSTRACT: Owing to changes in their chemistry and structure, polymers can be fabricated to demonstrate vastly different electrical conductivities over many orders of magnitude. At the high end of conductivity is the class of conducting polymers, which are ideal candidates for many applications in low-cost electronics. Here, we report the influence of the nature of the doping anion at high doping levels within the semi-metallic conducting polymer poly(3,4-ethylenedioxythiophene) (PEDOT) on its electronic transport properties. Hall effect measurements on a variety of PEDOT samples show that the choice of doping anion can lead to an order of magnitude enhancement in the charge carrier mobility > 3 cm^2/Vs at conductivities approaching 3000 S/cm under ambient conditions. Grazing Incidence Wide Angle X-ray Scattering, Density Functional Theory calculations, and Molecular Dynamics simulations indicate that the chosen doping anion modifies the way PEDOT chains stack together. This link between structure and specific anion doping at high doping levels has ramifications for the fabrication of conducting polymer-based devices. © 2017 The Authors. Journal of Polymer Science Part B: Polymer Physics Published by Wiley Periodicals, Inc. J. Polym. Sci., Part B: Polym. Phys. **2018**, *56*, 97–104

KEYWORDS: charge transport; conducting polymers; DFT; DFT calculations; GIWAXS; MD simulations; molecular dynamics; WAXS

INTRODUCTION Synthesis of polyacetylene[1] and polyaniline[2] has sparked the interest of many researchers over the past four decades to understand the charge transport mechanism(s) within conducting polymers. Factors on many different length scales within the polymeric material are considered important to the transport of charge, in turn then defining the conductivity of the polymer; chemical structure, oxidation level, conjugation length, and morphology, to name but a few. Despite ongoing studies to elicit new knowledge, the common understanding is that the properties of conducting polymers are dominated by the transport of holes (positive charges) along the conjugated network or "backbone" along the length of the polymer chain. This understanding leads to the classification of conducting polymers as p-type materials.

Through variation of the precursor monomer, fabrication process, and doping anion, many conducting polymers have been studied, such as polyaniline,[3] polypyrrole,[4] and poly(3,4-ethylenedioxythiophene) (PEDOT).[5] Chemical preparation of PEDOT doped with polystyrenesulfonate (PSS^-) has yielded conductivity of over 2000 S/cm by post-treatment (adding an ionic liquid[6] or treating with an acid[7] are two examples). Further increases in the conductivity to 3400 S/cm was achieved through use of (i) tosylate (Tos^-) as the doping anion, (ii) amphiphilic copolymers, and (iii) the vapor phase polymerization (VPP) process.[8] Adding to this, Gueye *et al*. used the post-treatment process with several solvents to enhance the Tos^- plus amphiphilic copolymer system yielding PEDOT conductivities of greater than 5000 S/cm.[9] Thiophene-based polymers have been employed in organic photovoltaics and other field effect devices owing to appreciable charge carrier mobility.[10] The study of Cho *et al*.[11] further pushed the electrical properties of PEDOT, by creating nanowires of single crystal PEDOT doped with Cl^- via VPP having electrical conductivity exceeding 7600 S/cm with a concomitant charge carrier mobility approaching 88 cm^2/Vs. In more detailed studies by Bubnova *et al.*,[12] the differences from the use of PSS^- or Tos^- were shown to arise

Additional Supporting Information may be found in the online version of this article.

from a transition in the conducting polymer from a Fermi glass to a semimetal respectively. Despite the demonstration of PEDOT in electrical applications from thermoelectronics[13] to spintronics[14] to energy storage,[15,16] no rationale has been provided to explain the role of the doping anion in achieving high electrical conductivity. Notably theoretical modelling, that is an essential and standard tool in many fields of material science, is to a large extend missing in conducting polymer research where the interpretation of experiments seldom relies on theoretical calculations. Recently, some of the present authors reported molecular dynamics (MD) simulations of morphology and crystallization of PEDOT with tosylate (Tos^-) as the doping anion.[17] At the same time, the theoretical understanding of the effect of different anions on electronic, structural, and morphological properties of the system at hand remains elusive and practically unexplored.

In this study, we report the electronic properties of conducting polymer PEDOT with respect to the doping anions using various experimental techniques [Hall measurements, photoabsorption, grazing incidence wide-angle X-ray scattering, X-ray Photoelectron Spectroscopy (XPS), and THz spectroscopy] combined with the theoretical modeling using atomistic MD simulations of material's morphology and the density functional theory (DFT) for calculations of electronic properties. Importantly this study focuses on high doping levels in excess of 50% (i.e., 1 anion for 2 EDOT monomers[16]), where the conducting polymer (in this case PEDOT) is said to be semimetallic.[12] This is in contrast to the majority of existing studies which are limited to the doping levels of 33% or less corresponding to pristine (i.e., as polymerized) PEDOT. A combination of the experimental characterization and theoretical simulations allowed us to outline the origin of the pronounced difference in transport properties of PEDOT with different anions, relating them to the differences in the morphology, which PEDOT exhibits when tosylate is substituted by different counterions.

EXPERIMENTAL

Sample Preparation

PEDOT was fabricated via VPP using $Fe(Tos)_3$ as the oxidant in a butanol/ethanol solvent mix, with and without added PEG-PPG-PEG amphiphilic triblock copolymer (2900 or 5800 Da Mw) (see Supporting Information). Chemically prepared PEDOT was prepared using polystyrene sulfonate or Tos^- as the doping anion, which was then spin-cast onto substrates.

Samples of the VPP PEDOT:Tos were then electrochemically reduced or oxidised by placing in a salt solution of $Na(NO_3)$, $Li(ClO_4)$, $Na_2(PhenylPO_4)$, NaCl, and Na(Tos), using the conducting polymer as the working electrode and a Pt wire as the counter electrode. A reducing potential of -1 V and oxidation potential of $+1$ V were applied to the samples.

Analysis

Hall effect measurements were made (Ecopus HMS-5300) using the van der Pauw configuration. Doping level of the anions were determined using a SPECS (SAGE, Phoibos 150-HSA) X-ray photoelectron spectroscope (XPS) fitted with a non-monochromated Al anode, power 200 W, with a base pressure of 2×10^{-6} Pa. For all anions except Tos, the survey scan was employed to determine the atomic percentage of the central atom of the anion (N, P, Cl). For all samples the atomic percentage of S was separated into S in Tos and S in EDOT by interpreting the S 2p fine scan. This is based on the peaks attributed to S 2p $^1/_2$ and S 2p $^3/_2$ in Tos and S 2p $^1/_2$ and S 2p $^3/_2$ in PEDOT (the two signals at 167–170 eV are from Tos, whereas those at 164–167 eV are from PEDOT). The doping level of anions per EDOT repeat unit (or number of EDOT repeat units per 1 anion) is calculated by summation of the atomic percentage of anions relative to S in EDOT. The full width at half maximum (FWHM) is 1.8 eV for all peaks fitted in the S 2p fine scans, except in the case of reduced PEDOT (1.5 eV) and when ClO_4^- is the secondary anion (1.6 eV).

Absorption spectra of PEDOT films coated over a glass substrate were obtained using an Agilent Technologies, Cary 5000 series UV–vis-NIR spectrometer. THz spectroscopy was conducted using the custom-built system described in ref. 18. Grazing Incidence Wide-Angle X-ray Scattering (GIWAXS) were performed with a setup[19] having a rotating Cu-anode as source, focused by a 1D multilayer mirror providing monochromatic X-ray radiation (Cu K-alpha, 1.5418 Å) at a grazing incident angle of $\sim$0.18°. The scattered radiation was collected with a Fuji imaging plate.

MD Simulations

MD Simulations were performed using General AMBER Force Field (GAFF)[20] employing the moltemplate code[21] in LAMMPS software suite.[22] Water molecules were described by a model of SPC/E.[23] 50 PEDOT chains with the oxidation levels corresponding to those measured by XPS as reported in Figure 1(c) were used in the calculations. We considered the chain length of PEDOT $N = 12$. Note that the chain length of PEDOT is not known exactly experimentally but is estimated to be in the range of $N = 10$–20 monomer units depending on the synthesis method employed.[24] It is also believed that short chains are obtained in polythiophenes by VPP according to the description by Yokozawa *et al.*[25] Additionally, a narrow and monodispersed molecular weight distribution is expected, which justifies the use of all of PEDOT chains with the same chain length in our simulation box. Finally, we note that that for the case of PEDOT:TOS the calculated morphology was shown to be rather insensitive to the chain length N.[17]

The corresponding number of Tos and anions to balance the charges of the system were considered in a proper proportion as measured by XPS (see Supporting Information Table S1 for the number of Tos and anios used). Then, the box is solvated with 30,000 water molecules. All the molecules were randomly placed in a computational box $12 \times 12 \times 12$ nm^3, which typically contained $\approx$101,000 atoms. The system was then minimized and equilibrated by 20 ns run of canonical *nVT* (at 293.15 K) ensemble using the Nose-Hoover thermostat[26] and the time integration method of

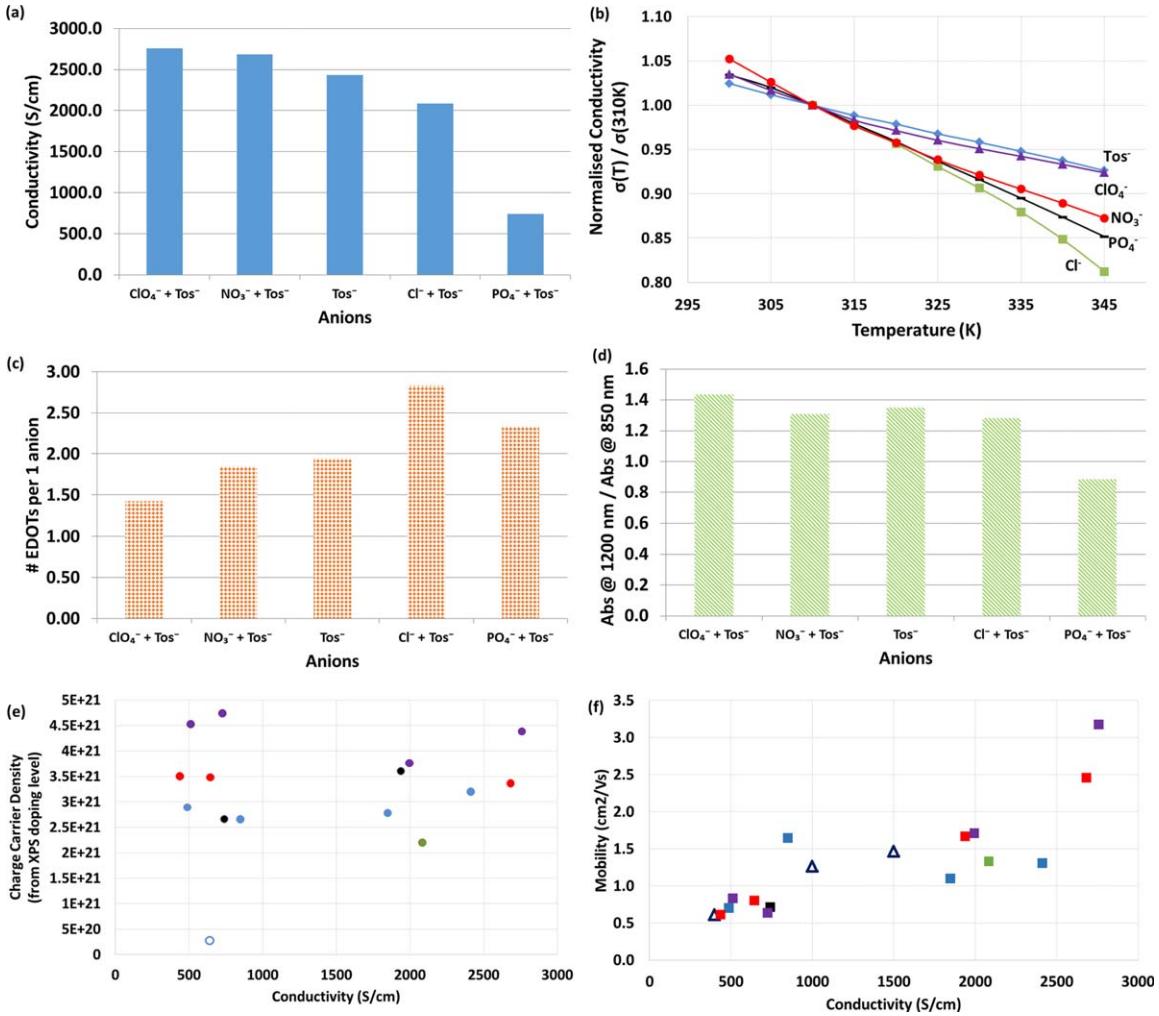

FIGURE 1 The influence of doping anion on VPP PEDOT properties. The (a) absolute electrical conductivity at room temperature, (b) normalized conductivity as a function of temperature, and (c) anion doping level for different anions in VPP PEDOT. (d) Ratio of the optical absorption at 1200 nm compared with 850 nm. Determination of (e) the charge carrier density and (f) the charge carrier mobility as a function of the electrical conductivity of the PEDOT variant from the Hall effect measurements and XPS. The open circle in (e) is an electrochemically reduced variant of VPP PEDOT. The open triangles in (f) are mobility and conductivity values determined from THz reflectance spectroscopy (optical measurement). For (b), (e), and (f) The PEDOT variants are initially doped with Tos^- and subsequently inserted with Tos^- (blue) ClO_4^- (purple), NO_3^- (red), Cl^- (green), and $PhenylPO_4^{-2}$ (black). [Color figure can be viewed at wileyonlinelibrary.com]

Verlet.[27] Then, water was consecutively removed in 7 steps, such as the water concentration was reduced approximately, from 82% w.t. (initial solution) to 70, 60, 43, 25, 16, 12, and finally 0% w.t. (i.e., a dry phase). The system was equilibrated in each step by a *npT* (at 1 atm and 293.15 K) ensemble for 10 ns run with both barostat and thermostat as Nose-Hoover with corresponding adjustment (decreasing) of its volume. Also, at each step, as a standard protocol, the simulations were performed until the potential energy of the system reached saturation. X-ray diffraction patterns were simulated as described by Coleman *et al.*[28] and implemented in LAMMPS suite[22] (see the Supporting Information for more details). Partial charges on each atom of PEDOT and Tos molecules were calculated using first-principles DFT functional WB97XD[29] with the 6–31 + g(d) basis set[30] as implemented in Gaussian 09, revision E.01 2009. The partial charge per atom were taken from the fitting to electrostatic potential population analysis as implemented in Gaussian suite.[31] Further details of the employed computational method can be found in ref. 17.

RESULTS

Charge transport in conducting polymers has been discussed with respect to holes (positive charges), and how they are created, stabilized, and traverse through the polymeric material.[32] Addition of counter-ions (anions) into the polymeric material, referred to as doping, allows for stabilisation of the hole through local charge neutralisation (attractive Coulomb force), thus increasing the lifetime of this charged state.[1] Electrochemical oxidation and reduction represents an efficient way to dope or de-dope the polymer by inserting or

removing anions from within the structure. In the case of PEDOT, insertion (removal) of anions leads to a lowering (increase) of visible light absorption (ca. 650 nm) with a concomitant increase (decrease) in the absorption of wavelengths above 750 nm. These changes in optical properties are observed for both polymeric chains in solution and thin film coatings thereof.[33] The visible absorption is associated with the "neutral" PEDOT chain having no holes along the conjugated chain. Insertion of anions to create holes leads to polarons being formed ($PEDOT^{+1}$, absorption ca. 791 and 1300 nm), with further insertion eventually leading to bipolarons ($PEDOT^{+2}$, absorption ca. 1170 nm; Supporting Information Figure S1). At high oxidation states, where a bipolaronic network is formed, the bipolaron and valence band begin to overlap, leading to the classification of the polymer as semimetallic in nature.[12,34]

Contrasting views have arisen in the literature about how the specific chemistry of the doping anion may or may not influence the charge transport. For example, (i) the doping anion (Tos^- vs. Cl^-) yielding no significant changes in electrical properties,[35] (ii) the doping anion (PSS^- vs. Tos^- vs. ClO_4^-) yielding orders of magnitude change in electrical properties,[36] (iii) to the replacement of PSS^- with Tos^- yielding a transition from semiconducting to semimetallic behavior.[12] To address these differences we herein demonstrate through experiment and calculation/simulation that transport properties in PEDOT may be attributed to the doping anion influencing the structure of the resultant PEDOT.

A variety of PEDOT samples were prepared, using VPP with the doping anion Tos^- and amphiphilic copolymer poly(ethylene glycol)-poly(propylene glycol)-poly(ethylene glycol) (PEG-PPG-PEG), and subsequently using ion-exchange to insert different anions. The ion-exchange process of the VPP PEDOT:Tos samples was achieved by subjecting samples to electrochemical reduction/oxidation cycling in an aqueous electrolyte solution of different anions (Tos^-, ClO_4^-, NO_3^-, Cl^-, $PhenylPO_4^{-2}$) to move anions in and out of the PEDOT, with a final oxidation step to insert as many of the anions as possible.

Figure 1 displays the electrical, optical and chemical analysis of the VPP PEDOT samples. Hall effect measurements were used to determine the electrical conductivity (σ, S/cm) for the respective samples, including the conductivity as a function of temperature. Combined with this is the optical (UV–vis-NIR) and chemical (XPS) analysis of the samples. Firstly, the chemical analysis revealed that the PEDOT samples had mixed doping, with both the original Tos^- from the VPP process and the new anion from the ion-exchange present in the PEDOT. Given the large reservoir of anions in the electrolyte for ion exchange, it was envisaged that the anion in solution would become the main dopant in the PEDOT. However, Tos^- appears to be well bound within the VPP PEDOT.

Comparison of VPP PEDOT with different anions inserted within the structure shows that the type of the inserted anion plays an important role on the resultant PEDOT properties [depicted in Figure 1(a) with respect to the electrical conductivity]. Firstly, the highest electrical conductivity across the samples is when ClO_4^- is employed, which is in agreement with several studies in the literature for chemically prepared and electropolymerised PEDOT.[36,37] Examination of the electrical conductivity as a function of temperature in Figure 1(b) shows all samples display metallic transport properties, similar to that shown for semimetallic PEDOT.[12] Inserting $PhenylPO_4^{-2}$ into the PEDOT yields an electrical conductivity one third that of the PEDOT:Tos reference sample. In part this is due to the $PhenylPO_4^-$ not doping to the same level as Tos^- (1 anion in 2.4 EDOTs vs. 1 in 1.8), as shown in Figure 1(c) (determined from XPS, see Supporting Information Figure S2). It is important to note that the very high doping level herein compared with that generally reported as the theoretical limit for PEDOT (1 anion in 3 EDOTs) is hypothesised to be related to coordination of anions with the triblock copolymer within the VPP PEDOT.[16] In direct comparison with $PhenylPO_4^{-2}$, the insertion of Cl^- yields a similar doping level to $PhenylPO_4^{-2}$ but a conductivity 2.5 times higher. Adding to this discussion is a comparison of the UV–vis-NIR spectra [Fig. 1(d) and Supporting Information Figure S3] for the ratio of absorption at 1200 nm compared with 850 nm. The observed ratio for ClO_4^- and NO_3^- in PEDOT is greater than the doping with $PhenylPO_4^{-2}$. Assigning this difference in ratio to changes in the levels of bipolarons and polarons present is ambiguous, given the overlap of their respective absorption (Supporting Information Figure S1). Understanding this variation is of further scientific research. However, this highlights that the specific nature of the anion influences the resultant VPP PEDOT properties, beyond those derived from different doping levels.

To investigate the relation of doping level and mobility with conductivity, a broader range of PEDOT samples were tested (chemically prepared and VPP). In the case of the VPP PEDOT samples, a different PEG-PPG-PEG copolymer was employed, and each sample respectively ion-exchanged with the aforementioned anions. The different fabrication (primarily owing to morphology changes as per ref. 8) and/or doping anions leads to markedly different electrical conductivity values. As shown in Figure 1(e) the number of charge carriers is relatively constant across these samples. The open circle data point represents an electrochemically reduced VPP PEDOT variant to demonstrate that deliberate removal of anions from PEDOT results in decreased numbers of charge carriers. The doping level from XPS (fine scan spectra shown in Supporting Information Figure S2) can be used to determine the approximate number of charge carriers per unit volume,[11] and by assuming no contribution of electrons to the charge transport the mobility of the holes can be calculated from the Hall effect measurements. In Figure 1(f) the order of magnitude increase in the mobility across these samples correlates with the respective order of magnitude increase in conductivity. In addition to Hall effect measurements combined with XPS to determine this relationship, THz spectroscopy was also employed to arrive at independent measurements of the optical conductivity, charge carrier

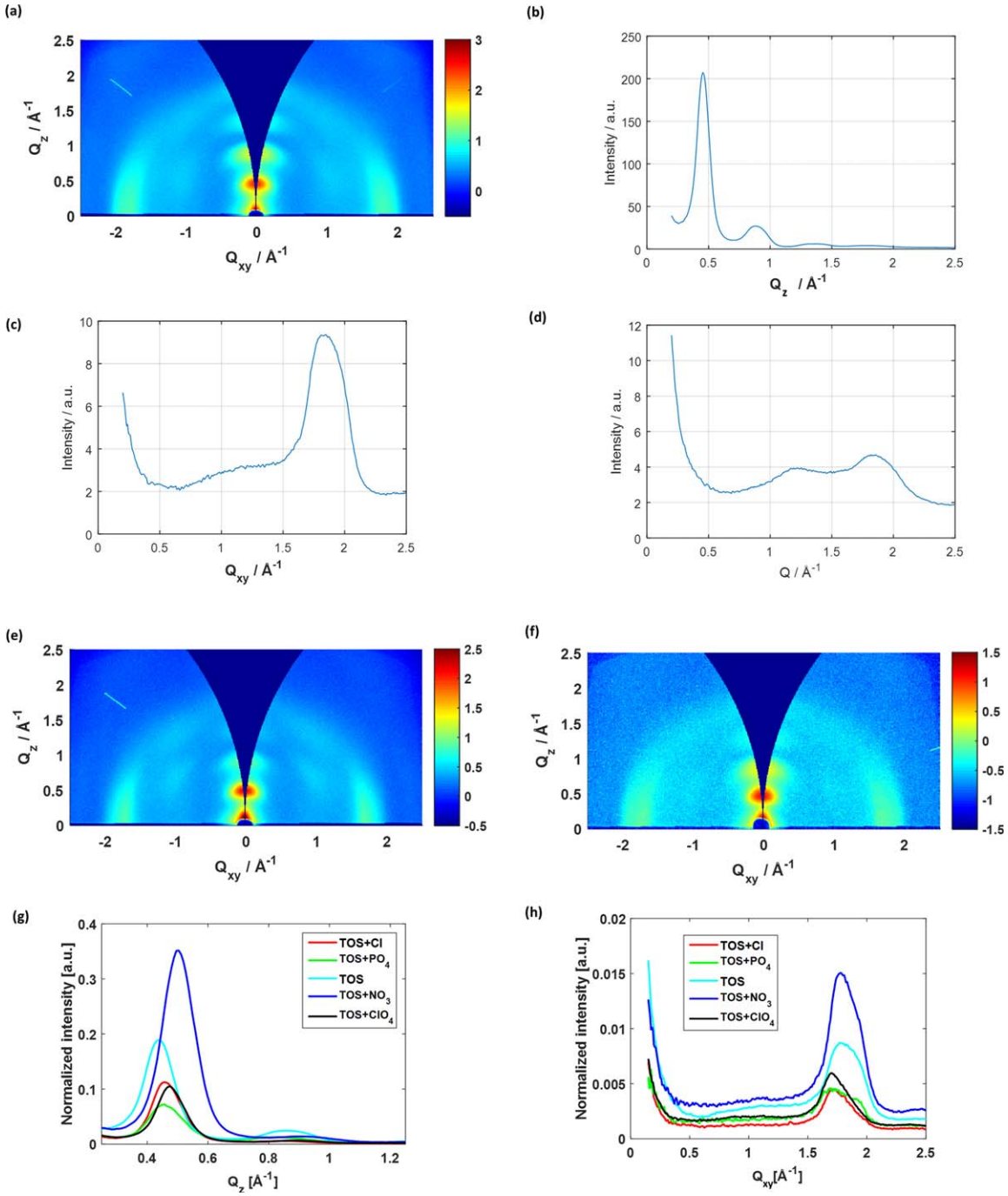

FIGURE 2 Structural analysis of mixed doped PEDOT at high doping levels. 2D grazing incident wide angle x-ray scattering spectra for (a) VPP PEDOT:Tos at high doping level after ion exchanged with Tos^-, and ion exchanged with (e) ClO_4^- and (f) PO_4^- for comparison. For the spectra in (a), the integrations (b) along the surface normal showing the *n00* lamellar peaks, (c) in the substrate plane, showing the *020* π-stacking peak, and (d) along the radial through the mixed index reflection are presented. (g,h) collate the integrations along the surface normal and substrate plane respectively, normalized to directly compare the anions studied herein. [Color figure can be viewed at wileyonlinelibrary.com]

density, and mobility (see Supporting Information Table S2, and as previously applied to PEDOT:PSS[18]). Figure 1(f) shows that the relationship between the optically derived transport properties overlay well with the electronically derived transport properties.

2D GIWAXS analysis (Fig. 2 and Supporting Information Fig. S4) provides information about the change in PEDOT chain ordering for the type of anion electrochemically inserted into the VPP PEDOT. All the samples exhibit pronounced crystallinity and are highly textured, with an "edge-on" orientation,

TABLE 1 The Determined *Q* Values and Corresponding *d*-Spacing for the PEDOT Structures Obtained using the Different Ion-Exchanged Anions

	[100]	[010]	mixed	[100]	[010]	mixed	
Anion	*d*-Spacing (Å)	*d*-Spacing (Å)	*d*-Spacing (Å)	*Qz* (1/Å)	*Qxy* (1/Å)	*Qxy* (1/Å)	*Qz* (1/Å)
Tos	14.3	3.5	5.2	0.44	1.82	1.07	0.57
Cl	13.7	3.6	5.9	0.46	1.75	0.95	0.5
ClO_4	13.1	3.6	5.3	0.48	1.73	0.99	0.65
NO_3	12.6	3.5	5.3	0.5	1.81	1	0.62
PhenylPO_4	13.7	3.6	5.5	0.46	1.76	0.95	0.63

that is, with lamellar stacking along the surface normal [Fig. 2(b)], and the π-stacking in the substrate plane [at Q_{xy} 1.75 $Å^{-1}$ in Fig. 2(c)]. The peak widths of the 100 (lamellar) and 020 (π-stack) reflections correspond to domain sizes of 5.5 and 2.5 nm along the surface normal and in the substrate plane, respectively, according to the Scherrer equation. The presence of "mixed-index" reflections at $(Q_{xy}, Q_z) = (1.0\ Å^{-1}, 0.6\ Å^{-1})$ in Figure 2(d) indicates that 3D structures are formed. All the ion exchanged samples exhibit even better ordering relative to as-prepared VPP PEDOT:Tos.

There is a correlation between the type of anion inserted into the VPP PEDOT and the lamellar spacing *d*. The *d*-spacing changes from 14.0 Å for the Tos^- samples to 12.6 Å for the ClO_4^- and NO_3^- counter-ions (see Table 1). The other anions of Cl^- and PhenylPO_4^{-2} are more similar to Tos^- (corroborating prior studies of ion exchange of Tos^- with Cl^- and vice versa,[38] and recent studies of VPP PEDOT:Tos treated with NaOH and HCl[39]). The anion influence on the structure correlates with the increased charge carrier mobility and electrical conductivity for the ClO_4^- and NO_3^- samples and varying levels of decreased conductivity for Cl^- and PhenylPO_4^{-2}.

MD simulations and DFT calculation were conducted to understand the role of the anion on PEDOT ordering and electronic structure. Firstly, it is important to note that due limitations of the calculations and simplification of the computational model, they are unlikely to describe all the subtle features seen in the experimental observations. Secondly, the DFT calculations for the molecular orbitals (MOs) and DOSs for a single chain with one anion (polaron) or two chains in a π-stacking orientation with two anions (bipolaron) show no differences between different counterions (Supporting Information Figure S5 and S6). That is to say, the type of anion has no influence on the electronic band structure of the PEDOT when the geometric arrangement is held constant.

However, MD simulations for the highly doped PEDOT show that the morphology of the systems at hand strongly depends on the type of anions and the doping level. The simulations were conducted in absence of a hard substrate (which possibly induces strong texturing in "edge-on" orientation). This is a likely scenario for the VPP process, where nanofilms of polymer are formed at the liquid-vapor interface many micrometers away from the hard substrate. Figure 3(a) shows representative snapshots of the PEDOT structure illustrating formation of crystallites embedded in an amorphous matrix. The calculated X-ray diffraction pattern for all anions, Figure 3(e), shows a broad main peak at $Q = 1.75\ Å^{-1}$ confirming the formation of crystallites of the size of 14–16 Å with the interchain distance $d = 3.45$ Å. These values are in reasonable agreement with the experimental GIWAXS measurements [Fig. 2(g,h) and Supporting Information S4), in line with the widely reported packing structure for PEDOT.

The structure of crystallites observed in the MD simulation is, however, strikingly different depending on the anion type and charge concentration. For the case of not too high doping level, $\leq$50% (corresponding to the cases of Tos^-/Cl^-, Tos^-/PO_4^-), the crystallites are composed of π-π stacked PEDOT chains, with anions distributed randomly around the crystallites [Fig. 3(b)]. For the case of very high doping levels, $\geq$ 50% (corresponding to the cases of Tos^-, Tos^-/NO_3^-, and Tos^-/ClO_4^-) the morphology of crystallites undergoes transformation with doping anions intercalating between PEDOT chains to form a "sandwich" structure to screen the positive charges in PEDOT chains. Interestingly, only planar anions (Tos^- and NO_3^-) intercalate between PEDOT chains [Fig. 3(c)] whereas tetrahedral-shaped anions ClO_4^- cannot penetrate the space between PEDOT chains and thus stay outside crystallites [Fig. 3(d)]. The formation of the intercalated structure is reflected in the radial distribution function $g_{P\text{-}P}(r)$ for the carbon atoms describing the distance between PEDOT chains, see Figure 3(e). For the cases of Tos^-/Cl^-, Tos^-/PhenylPO_4^{-2} (when no intercalating structure forms) $g_{P\text{-}P}(r)$ shows peaks at integer values of $r/r_{\pi\text{-}\pi}$ where the peak $r/r_{\pi\text{-}\pi} = 1$ corresponds to the π-π distance between PEDOT chains, $r_{\pi\text{-}\pi} = 3.45$ Å. For the remaining systems (Tos^-, Tos^-/NO_3^-, and Tos^-/ClO_4^-) where the intercalating structure forms, the peak at $r/r_{\pi\text{-}\pi} = 1$ is absent and the first peak in $g_{P\text{-}P}(r)$ corresponds to $r/r_{\pi\text{-}\pi} = 2$. Note that for the case of Tos^-/ClO_4^- only Tos counterions intercalate between the PEDOT chains. A signature of the intercalated structure is seen in the predicted X-ray scattering [Fig. 3(d)] at $Q = 0.95\ Å^{-1}$ corresponding to the double π-π stacking distance $2r_{\pi\text{-}\pi} = 7$ Å. Note that the shoulder at $Q = 0.95\ Å^{-1}$ is apparently not seen for either Cl^- or PhenylPO_4^{-2}. Figure 3(g,h) show distance distribution between the anions and PEDOT chains.

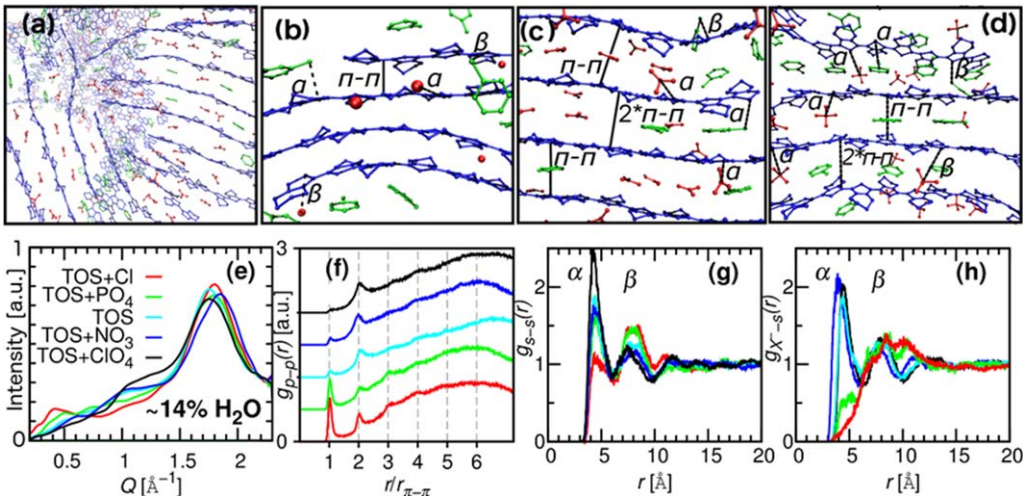

FIGURE 3 MD simulation of the PEDOT chain ordering for mixed anions at high doping levels. (a) MD Snapshot the PEDOT: Tos^-/NO_3^- structures. PEDOT is shown in blue, Tos^- is green, Cl^- and NO_3^- in red [water molecules, H atoms from PEDOT and Tos^- and O atoms and methyl groups from Tos^- are not shown for clarity in (a–d)]. The snap-shot corresponds to a zoomed view of a representative region of a computational box containing PEDOT crystallite, where a direction of a view is chosen perpendicular to the crystallite to clearly see the intercalation effect. (b–d) Rendered images of PEDOT crystallites for the cases of Tos^-/Cl^-, Tos^-/NO_3^-, and Tos^-/ClO_4^- counterions, respectively. Stacking distances $r_{\pi\text{-}\pi} = 3.45$ Å and $2r_{\pi\text{-}\pi}$ are indicated. "α" and "β" indicate counterions contributing to corresponding peaks in (g and h). (c and d) correspond to the intercalated ("sandwich") morphology. (e) X-ray Diffraction Patterns for different counterions. Radial distribution functions: (f) $g_{P\text{-}P}(r)$ for the distance between PEDOT chains. (g) $g_{S\text{-}S}(r)$ for the distance between SO_3^- from Tos^- and Sulfur from PEDOT. (h) $g_{X^-\text{-}S}(r)$ for the distance between center of mass of anion and Sulfur from PEDOT. For all figures water content is 14% w/w. [Color figure can be viewed at wileyonlinelibrary.com]

For all anions, except Cl^- and PhenylPO_4^{-2} this distribution shows similar features and is peaked at the distances ~4 and ~8 Å (peaks β and α, respectively). These peaks correspond to anions situated on the side of chains as well as between (or above/below) the chains, see Figure 3(b–d) for illustration. These features cannot be unambiguously assigned as an effect of intercalation in GIWAXS patterns, however. GIWAXS simulation of the highly crystalline structure reported by Kim and Bredas[40] also reveals features at $Q_{xy} = 1.1$ Å^{-1} (Supporting Information Figure S7). Further structural investigation is necessary to validate the hypothesis arising from the MD simulations at high doping levels of $\geq 50\%$.

CONCLUSIONS

In summary, the doping anion plays a critical role in defining the electronic transport properties of PEDOT. When ClO_4^- is introduced into the structure to form PEDOT:Tos/ClO_4 the electrical conductivity approaches 3000 S/cm with a mobility of > 3 cm^2/Vs. While the molecular orbitals and nature of the charge carriers in PEDOT chains do not alter, at high doping levels the specific anion chosen leads to changes in the morphological structure of PEDOT. GIWAXS indicates highly ordered PEDOT chains, while MD simulations give insight that certain anions may actually intercalate into the π-π stacking of PEDOT. Enhancement of the charge carrier mobility towards that of metals, as well as the crystallinity, are critical to realizing the uptake of conducting polymers such as PEDOT in low-cost, flexible electronic devices.

ACKNOWLEDGMENTS

The authors acknowledge the European Research Council (ERC-starting-grant 307596), the Swedish foundation for strategic research (project: "Nano-material and Scalable TE materials"), the Knut and Alice Wallenberg foundation (project "Power Paper" and "Tail of the Sun"), The Swedish Energy Agency (38332 − 1), the Swedish Research Council via "Research Environment grant" on "Disposable paper fuel cells" (2016 − 05990), and the Advanced Functional Materials Center at Linköping University. The authors thank Masatsugu Yamashita from the THz Sensing & Imaging Lab at RIKEN in Japan for conducting the THz reflectance spectroscopy experiments. D.R. Evans acknowledges the support of the Australian Research Council through the Future Fellowship scheme (FT160100300). J.W. Andreasen acknowledges the support of the European Research Council (ERC-consolidator-grant 681881). The computations were performed on resources provided by the Swedish National Infrastructure for Computing (SNIC) at NSC.

REFERENCES AND NOTES

1 C. Chiang, C. Fincher, Jr., Y. Park, A. Heeger, H. Shirakawa, E. Louis, S. Gau, A. G. MacDiarmid, *Phys. Rev. Lett.* **1977**, *39*, 1098.

2 Y. Cao, G. M. Treacy, P. Smith, A. J. Heeger, *Appl. Phys. Lett.* **1992**, *60*, 2711.

3 S. J. Pomfret, P. N. Adams, N. P. Comfort, A. P. Monkman, *Adv. Mater.* **1998**, *10*, 1351.

4 M. Yamaura, T. Hagiwara, K. Iwata, *Synth. Met.* **1988**, *26*, 209.

5 (a) M. Fabretto, C. Jariego-Moncunill, J. P. Autere, A. Michelmore, R. D. Short, P. Murphy, *Polymer.* **2011**, *52*, 1725; (b) D. C. Martin, J. Wu, C. M. Shaw, Z. King, S. A. Spanninga, S. Richardson-Burns, J. Hendricks, J. Yang, *Polym. Rev.* **2010**, *50*, 340.

6 C. Badre, L. Marquant, A. M. Alsayed, L. A. Hough, *Adv. Func. Mater.* **2012**, *22*, 2723.

7 Y. Xia, K. Sun, J. Ouyang, *Adv. Mater.* **2012**, *24*, 2436.

8 M. V. Fabretto, D. R. Evans, M. Mueller, K. Zuber, P. Hojati-Talemi, R. D. Short, G. G. Wallace, P. J. Murphy, *Chem. Mater.* **2012**, *24*, 3998.

9 M. N. Gueye, A. Carella, N. Massonnet, E. Yvenou, S. Brenet, J. Faure-Vincent, S. Pouget, F. Rieutord, H. Okuno, A. Benayad, *Chem. Mater.* **2016**, *28*, 3462.

10 (a) Y. Li, Y. Zou, *Adv. Mater.* **2008**, *20*, 2952; (b) I. McCulloch, M. Heeney, C. Bailey, K. Genevicius, I. MacDonald, M. Shkunov, D. Sparrowe, S. Tierney, R. Wagner, W. Zhang, *Nat. Mater.* **2006**, *5*, 328.

11 B. Cho, K. S. Park, J. Baek, H. S. Oh, Y.-E. Koo Lee, M. M. Sung, *Nano Lett.* **2014**, *14*, 3321.

12 O. Bubnova, Z. U. Khan, H. Wang, S. Braun, D. Evans, M. Fabretto, P. Hojati-Talemi, D. Dagnelund, J.-B. Arlin, Y. Geerts, S. Desbief, D. Breiby, J. W. Andreasen, R. Lazzaroni, W. Chen, I. Zozoulenko, M. Fahlman, P. Murphy, M. Berggren, X. Crispin, *Nat. Mater.* **2014**, *13*, 190.

13 (a) O. Bubnova, Z. U. Khan, A. Malti, S. Braun, M. Fahlman, M. Berggren, X. Crispin, *Nat. Mater.* **2011**, *10*, 429; (b) T. Park, C. Park, B. Kim, H. Shin, E. Kim, *Energy Environ. Sci.* **2013**, *6*, 788.

14 K. Ando, S. Watanabe, S. Mooser, E. Saitoh, H. Sirringhaus, *Nat. Mater.* **2013**, *12*, 622.

15 (a) B. Winther-Jensen, O. Winther-Jensen, M. Forsyth, D. R. MacFarlane, *Science.* **2008**, *321*, 671; (b) P. Cottis, D. Evans, M. Fabretto, S. Pering, P. J. Murphy, P. Hojati-Talemi, *RSC Adv.* **2014**, *4*, 9819.

16 C. Karlsson, J. Nicholas, D. Evans, M. Forsyth, M. Strømme, M. Sjödin, P. C. Howlett, C. Pozo-Gonzalo, *ChemSusChem.* **2016**, *9*, 2112.

17 J. F. Franco-Gonzalez, I. V. Zozoulenko, *J. Phys. Chem. B.* **2017**, *121*, 4299.

18 M. Yamashita, C. Otani, M. Shimizu, H. Okuzaki, *Appl. Phys. Lett.* **2011**, *99*, 143307.

19 D. Apitz, R. Bertram, N. Benter, W. Hieringer, J. W. Andreasen, M. M. Nielsen, P. Johansen, K. Buse, *Phys. Rev. E.* **2005**, *72*, 036610.

20 J. Wang, R. M. Wolf, J. W. Caldwell, P. A. Kollman, D. A. Case, *J. Comput. Chem.* **2004**, *25*, 1157.

21 A. I. Jewett, Z. Zhuang, J.-E. Shea, *Biophys. J.* **2013**, *104*, 169a.

22 S. Plimpton, *J. Comput. Phys.* **1995**, *117*, 1.

23 H. Berendsen, J. Postma, W. Van Gunsteren, J. Hermans, In *The Jerusalem Symposia on Quantum Chemistry and Biochemistry*, B. Pullman, Ed.; Springer: Dordrecht, April **1981**; Vol. *14*, pp 13.

24 (a) A. Ugur, F. Katmis, M. Li, L. Wu, Y. Zhu, K. K. Varanasi, K. K. Gleason, Adv. Mater. **2015**, *27*, 4604; (b) A. Elschner, S. Kirchmeyer, W. Lovenich, U. Merker, K. Reuter, *PEDOT: Principles and applications of an intrinsically conductive polymer*; CRC Press: Florida, **2010**.

25 T. Yokozawa, A. Yokoyama, *Chem. Rev.* **2009**, *109*, 5595.

26 (a) W. Shinoda, M. Shiga, M. Mikami, *Phys. Rev. B.* **2004**, *69*, 134103; (b) G. J. Martyna, D. J. Tobias, M. L. Klein, *J. Chem. Phys.* **1994**, *101*, 4177; (c) M. Parrinello, A. Rahman, *J. Appl. Phys.* **1981**, *52*, 7182.

27 M. E. Tuckerman, J. Alejandre, R. López-Rendón, A. L. Jochim, G. J. Martyna, *J. Phys. A: Math. Gen.* **2006**, *39*, 5629.

28 S. Coleman, D. Spearot, L. Capolungo, *Modell. Simul. Mater. Sci. Eng.* **2013**, *21*, 055020.

29 Y.-S. Lin, G.-D. Li, S.-P. Mao, J.-D. Chai, *J. Chem. Theory Comput.* **2012**, *9*, 263.

30 R. Krishnan, J. S. Binkley, R. Seeger, J. A. Pople, *J. Chem. Phys.* **1980**, *72*, 650.

31 U. C. Singh, P. A. Kollman, *J. Comput. Chem.* **1984**, *5*, 129.

32 J. L. Bredas, G. B. Street, *Acc. Chem. Res.* **1985**, *18*, 309.

33 J. J. Apperloo, L. B. Groenendaal, H. Verheyen, M. Jayakannan, R. A. J. Janssen, A. Dkhissi, D. Beljonne, R. Lazzaroni, J.-L. Brédas, *Chem. Eur. J.* **2002**, *8*, 2384.

34 W. A. Munoz, S. K. Singh, J. Franco-Gonzalez, M. Linares, X. Crispin, I. Zozoulenko, *Phys. Rev. B.* **2016**, *94*, 205202.

35 B. Winther-Jensen, M. Forsyth, K. West, J. W. Andreasen, P. Bayley, S. Pas, D. R. MacFarlane, *Polymer* **2008**, *49*, 481.

36 G. Zotti, S. Zecchin, G. Schiavon, F. Louwet, L. Groenendaal, X. Crispin, W. Osikowicz, W. Salaneck, M. Fahlman, *Macromolecules* **2003**, *36*, 3337.

37 P.-H. Aubert, L. Groenendaal, F. Louwet, L. Lutsen, D. Vanderzande, G. Zotti, *Syn. Met.* **2002**, *126*, 193.

38 B. Winther-Jensen, M. Forsyth, K. West, J. W. Andreasen, G. G. Wallace, D. R. MacFarlane, *Org. Electron.* **2007**, *8*, 796.

39 Z. U. Khan, O. Bubnova, M. J. Jafari, R. Brooke, X. Liu, R. Gabrielsson, T. Ederth, D. R. Evans, J. W. Andreasen, M. Fahlman, *J. Mater. Chem. C.* **2015**, *3*, 10616.

40 E. G. Kim, J. L. Brédas, *J. Am. Chem. Soc.* **2008**, *130*, 16880.